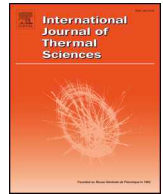




ELSEVIER

Contents lists available at ScienceDirect

International Journal of Thermal Sciences

journal homepage: www.elsevier.com/locate/ijts

Numerical analysis and parametric optimization on flow and heat transfer of a microchannel with longitudinal vortex generators

Jian-Fei Zhang^{a,*}, Long Jia^a, Wei-Wei Yang^a, Jan Taler^b, Pawel Oclon^b

^a Key Laboratory of Thermo-Fluid Science and Engineering of MOE, School of Energy and Power Engineering, Xi'an Jiaotong University, Xi'an, 710049, China

^b Institute of Thermal Power Engineering, Faculty of Mechanical Engineering, Cracow University of Technology, Cracow, Poland

ARTICLE INFO

Keywords:

Microchannel
Longitudinal vortex generators
Heat-transfer enhancement
Optimization
Taguchi method
Second-order multiple regression model

ABSTRACT

In this paper, a three dimensional (3D) numerical model of a rectangular microchannel with longitudinal vortex generators (LVGs) is developed. The impacts of length, width, longitudinal spacing, and number of LVG pairs are discussed. To improve the flow and heat-transfer performance, the Taguchi method is employed for optimization. Three evaluation indexes—Nusselt number (Nu), Fanning friction factor (f), and overall efficiency (η)—are selected. The analysis of the influence degree of the geometric parameters of LVGs are carried out by intuitive analysis of the Taguchi method results, and the optimum combinations of geometric parameters are also determined. Also, the second-order dimensionless correlations involving multiple impact factors are obtained through response surface analysis. Results show that the number and longitudinal spacing of LVG pairs are the main impact factors for Nu . Regarding the flow resistance, the number and length of LVGs have a much stronger influence than other parameters. Two optimum combinations for Nu and overall efficiency are acquired, which achieve a 23.6% and 7.2% increase for Nu and overall efficiency, respectively, compared with the original model. The maximum differences between the correlations and test models are less than 15% for all of the evaluation indexes. The present investigation can be beneficial for the design and optimization of LVGs-enhanced microchannel heat sinks.

1. Introduction

With the rapid development of micro-electro-mechanical systems (MEMSs), fluid flow and heat transfer at the micro-scale have been the focus of many researchers. Owing to their small size, MEMSs have high heat flux, which imposes a higher requirement for the system's heat-transfer characteristics. Since Tuckerman and Pease [1] first applied a rectangular microchannel to a new heat sink as an effective way to enhance heat transfer, allowing a high power density, microchannels have been studied by numerous researchers, including their application in single-phase forced-flow cooling [2–4], two-phase cooling [5,6]. To improve the performance of the microchannel, many researchers have done a lot of research on the optimization of the microchannel heat sink. Wang et al. [7] numerically optimized the geometric parameters of the microchannel heat sink, including channel number, aspect ratio, and width ratio of the channel to pitch while nanofluid was as the coolant. Lin et al. [8] developed a wavy microchannel heat sink with changing wavelength along the flow direction. The numerical investigation shows that the new design has a better thermal performance than the straight and the original wavy microchannel. Chuan et al. [9]

proposed an innovative concept which replacing solid fins by porous fins in the microchannel heat sink to reduce flow resistance. They found that compared with the conventional heat sink, the porous fins make 43.0%–47.9% pressure drop decrease while the price is less than 5% increase of thermal resistance under the simulation conditions in this paper. In addition, some researchers designed and developed the double-layered microchannel heat sinks [10–12] which have better heat dissipation performance.

Although smooth microchannels can be applied to cooling in high-power-density devices, to achieve a higher cooling performance, circular [13,14] and square [15,16] micro-pin fin arrays have been applied in microchannels. However, longitudinal vortex generators (LVGs) [17], which can generate longitudinal vortices and effectively disturb the flow boundary layer, have been widely used in heat exchangers or heat-transfer units of conventional scale [18–20]. Thus, the technology of incorporating LVGs into microchannels is deemed to be another effective way of improving heat-transfer performance. Some researchers experimentally and numerically investigated the thermo-hydraulic performance of LVGs in the microchannel and optimized the structure of LVGs by the parametric study. Liu et al. [21] conducted

* Corresponding author.

E-mail address: zhangjf@mail.xjtu.edu.cn (J.-F. Zhang).

<https://doi.org/10.1016/j.ijthermalsci.2019.03.036>

Received 4 November 2018; Received in revised form 1 February 2019; Accepted 27 March 2019

1290-0729/ © 2019 Elsevier Masson SAS. All rights reserved.

Nomenclature*List of Symbols*

A_{ch}	Base area of the microchannel, m^2
b	Width of LVGs, m
CR	Contribution ratio
c_p	Specific heat $kJ \cdot (kg \cdot K)^{-1}$
D_h	Hydraulic diameter, m
f	Fanning friction factor
H	Height of channel, m
h	Heat-transfer coefficient $W \cdot (m^2 \cdot K)^{-1}$
k	Thermal conductivity $W \cdot (m \cdot K)^{-1}$
L	Length of channel, m
l	Length of LVGs, m
N	Number of LVG pairs
Nu	Nusselt number
Δp	Pressure drop, Pa
p	Static pressure, Pa
Re	Reynolds number
ΔT	Temperature differences, K
T	Temperature, K
S_l	Longitudinal spacing of two LVGs, m

S_t	Distance between two adjacent LVG pairs, m
SNR	Signal-to-noise ratio
U_{in}	Inlet velocity, $m^2 s^{-1}$
W	Width of the microchannel, m

Greek symbols

ϕ	Generalized variable
β	Attack angle of LVGs, rad
η	Overall efficiency
μ	Dynamic viscosity, Pa·s
ρ	Density, $kg \cdot m^{-3}$
Γ_ϕ	Generalized diffusion coefficients
S_ϕ	Generalized source term

Subscripts

avg	Value of average
in	Inlet
max	Value of maximum
out	Outlet
s	Smooth channel

experimental investigations on the liquid-flow and heat-transfer performance in rectangular microchannels with LVGs, and considered the influence of number, attack angle, and arrangement of LVGs. They found that LVGs can decrease the critical Reynolds number compared to a smooth microchannel. The results show that the LVG-enhanced microchannel increased the heat-transfer performance by 9%–21% for laminar flow and by 39%–90% for turbulent flow compared with a smooth microchannel with the Reynolds numbers varying from 170 to 1200. Based on Liu's study, Chen et al. [22] experimentally investigated the impact of the aspect ratio of microchannels and the number and height of LVG pairs. They found that the lower the aspect ratio of the microchannel and height of the LVGs, the more heat-transfer performance was increased. These results indicate that the critical Reynolds number increases with the reduction of the number of LVG pairs. Ebrahimi et al. [23] numerically studied heat-transfer and flow characteristics in microchannels with different arrangements of LVG pairs and found that microchannels equipped with LVGs increased heat-transfer performance by 2%–25% compared to smooth microchannels with the Reynolds numbers varying from 100 to 1100. Datta et al. [24] conducted numerical heat-transfer and flow-processes studies in microchannels with different LVG attack angles and reported that LVGs with a 30° attack angle for Reynolds numbers greater than 600 showed the best overall performance and, further, that a larger channel length downstream of the second LVG pair enhanced heat transfer. In Ref. [25], Datta et al. used the genetic algorithms and obtained the expression of Nusselt number, friction factor involving Reynolds number and location of vortex generator. The predicted model shows that compared with the smooth channel, the vortex generator increased the heat-transfer performance by 40–135% while the pressure drop increased by 62–186.7% with the increase of Reynold number. Zhang et al. [26] were the first to apply LVGs to micro-gaps of three-dimensional (3D) stacked chips. They numerically investigated the flow and heat-transfer performance of micro-gaps with LVGs and considered the influence of different arrangement parameters. Their results indicate that decreasing transverse spacing and increasing height of micro-gaps and number of LVG pairs can enhance heat transfer. The overall performance of micro-gaps equipped with LVGs could, therefore, be better than that with smooth micro-gaps.

As mentioned above, LVGs can effectively enhance the heat-transfer performance in microchannels, and many investigators have studied the

impact of microchannel structures and arrangements of LVG pairs. However, in these studies, control variable method is widely used, and attack angle and number of LVGs are the main objects of investigation. Moreover, there are few available studies focused on the influence degree and optimum combinations of LVG structure parameters in the microchannel. In addition, thermo-hydraulic performance correlations showing the impact of LVGs parameters have yet to be presented with respect to microchannels. The expressions obtained by Ref. [25] only considered the influence of the LVGs arrangement and Reynolds number while the impact of LVGs structure themselves such as length and width are not considered.

In this paper, the effect of the length, width, longitudinal spacing, and number of LVGs on the flow and heat transfer characteristics of microchannels is numerically investigated. The influence mechanism of LVGs geometric parameters is analyzed. Furthermore, the Taguchi method [27] is employed to determine the influence degree of different parameters and optimized combinations of different parameters for heat-transfer and overall performance. Moreover, the second-order multiple regression models are set up by response surface methodology (RSM) and thermo-hydraulic performance correlations of Nusselt number, friction factor, and overall efficiency are presented, considering the impact of four LVG geometric parameters and Reynolds number. The results shown in this paper are meaningful for the engineering application of flow and heat transfer in microchannels.

2. Model description and numerical method

2.1. Physical and computational model

A schematic of a rectangular microchannel with LVGs is shown in Fig. 1. The length, width, and height of the microchannel, shown in Fig. 1(a), are 20, 1.5, and 0.1 mm, respectively. Fig. 1(b) shows the geometric parameters of LVGs; that is, l , b , and β are the length, width, and attack angle of the LVGs, respectively. According to the results on LVGs investigated by Leu et al. [28] and Wu and Tao [29,30], LVGs with an attack angle of 45° provided the best heat-transfer enhancement. Therefore, in this paper, β is set at 45°. S_l represents the longitudinal spacing of symmetrical LVG pairs and S_t the distance between two adjacent LVG pairs. In the present work, the impacts of varying the structure (l , b , S_l) and the number (N) of LVGs are the main objects of

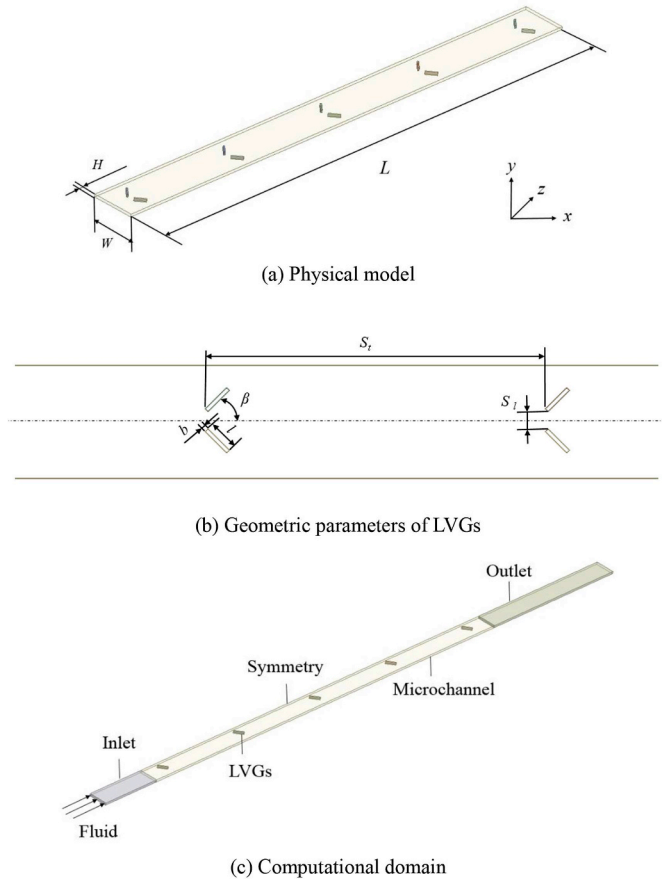


Fig. 1. Schematic of microchannel of LVGs: (a) physical model, (b) geometric parameters of LVGs, and (c) computational domain.

investigation, while the dimensions of the microchannel remain the same. Owing to the symmetric arrangement of the microchannel and LVGs, the computational domain, which is shown in Fig. 1(c), can be reduced to half of the microchannel.

2.2. Mathematical description

In this study, we focused on the single-phase laminar flow and heat-transfer characteristics of microchannels. Deionized water was used as the working fluid with an inlet temperature of 298 K and assumed incompressible. Silicon (Si) was selected as the LVG material. The temperature-dependent thermo-physical properties of deionized water and Si are shown in Table 1. The governing equations include mass, momentum, and energy equations. The general form of them can be written as follow:

$$\frac{\partial(u\phi)}{\partial x} + \frac{\partial(v\phi)}{\partial y} + \frac{\partial(w\phi)}{\partial z} = \frac{\partial}{\partial x} \left(\Gamma_\phi \frac{\partial\phi}{\partial x} \right) + \frac{\partial}{\partial y} \left(\Gamma_\phi \frac{\partial\phi}{\partial y} \right) + \frac{\partial}{\partial z} \left(\Gamma_\phi \frac{\partial\phi}{\partial z} \right) + S_\phi \quad (1)$$

The variables used in differential equations are shown in Table 2.

To describe the flow and heat-transfer characteristics well, some parameters are defined as follows. The Reynolds number (Re) is defined as

$$Re = \frac{\rho U_{in} D_h}{\mu_{in}} \quad (2)$$

where

$$D_h = \frac{2WH}{W+H} \quad (3)$$

The Nusselt number mentioned in this paper is the average Nusselt number which is calculated by using the following correlation,

$$Nu = \frac{hD_h}{k_m} \quad (4)$$

where

$$h = \frac{q}{\Delta T} \quad (5)$$

$$q = \dot{m}c_p(T_{out} - T_{in})/A_{ch} \quad (6)$$

The Fanning friction factor is adopted to represent the resistance and is defined as

$$f = \frac{D_h \Delta p}{2L\rho U_{in}^2} \quad (7)$$

2.3. Numerical method and boundary condition

In this study, Fluent 17.0 was employed to simulate the fluid-flow and heat-transfer processes. The solution method was based on the SIMPLE algorithm, and the second-order upwind scheme was adopted to discretize the convection term. The convergence conditions were defined as follows: the residuals of the energy equation and other equations were less than 10^{-8} and 10^{-6} , respectively. In the present computational model, the channel wall thickness was neglected. All the interfaces between the wall and the fluid were under no-slip boundary conditions, and the side walls and top wall were adiabatic. The symmetry plane was under the symmetric boundary condition. The temperature of the bottom wall remained 323.15 K. The inlet velocity was considered to be uniform. The boundary conditions for the temperature and the velocity at the outlet are shown as follow,

$$\text{for velocity, } \frac{\partial u}{\partial z} = \frac{\partial v}{\partial z} = \frac{\partial w}{\partial z} = 0 \quad (8)$$

$$\text{for temperature, } \frac{\partial T}{\partial z} = 0 \quad (9)$$

2.4. Grid independency and model verification

Non-uniform grids were generated by ANSYS meshing based on the sweep method. The inflation layer, a local mesh encryption method, was applied to the near-wall grids. Four grids with different mesh densities were generated to carry out the grid independence test. The results of the Nusselt number and pressure drop for different grids at $U_{in} = 2.28$ m/s, $Re = 482$ are shown in Table 3. There was little difference (less than 1%) in the results between the third and fourth grids, while the mesh number increased by 55%. Thus, the third grid was chosen for the simulation.

To validate the grid and numerical simulation method, a geometry with the same structure as the ‘‘G2’’ model in Ref. [21] was established. In ‘‘G2’’ model, the length (L), width (b), attack angle (β) and the number (N) of LVGs are 0.4 mm, 0.05 mm, 45° and 5, respectively. And the longitudinal spacing of symmetrical LVG pairs (S_1) is 0.2 mm. Fig. 3 shows the data of the present numerical simulation and that of Liu et al. [21]. As shown in Fig. 2, the maximum deviations of the Nusselt

Table 1

Temperature-dependent thermo-physical properties of silicon and Deionized-water [18].

Properties	Silicon	Deionized-water
μ (Pa·s)	/	$0.0194-1.065 \times 10^{-4}T + 1.489 \times 10^{-7}T^2$
k (W/(m·K))	$290-0.4T$	$-0.829 + 0.0079T - 1.04 \times 10^{-5}T^2$
c_p (J/(kg·K))	$390 + 0.9T$	$5348-7.42T + 1.17 \times 10^{-2}T^2$
ρ (kg/m ³)	2330	998.2

Table 2
Variables in different equations.

Equations	ϕ	Γ_ϕ	S_ϕ
mass	1	0	0
x-momentum	u	μ/ρ	$-1/\rho \partial p/\partial x$
y-momentum	v	μ/ρ	$-1/\rho \partial p/\partial y$
z-momentum	w	μ/ρ	$-1/\rho \partial p/\partial z$
Energy (Fluid)	T	$k/(\rho c_p)_{\text{fluid}}$	0
Energy (Solid)	T_{solid}	k_{solid}	0

Table 3
Grid independency.

Mesh number/ 10^4 (grid size)	$U_{\text{in}} = 2.288$ m/s, Reynolds number 482 $l = 400$ μm , $b = 50$ μm , $S_1 = 200$ μm , $N = 5$	Nu	Differences/%	$\Delta p/\text{Pa}$	Differences/%
100 (0.08 mm)		6.104	17.4	71404.9	3.5
149 (0.05 mm)		7.572	2.5	73287.75	0.97
194 (0.03 mm)		7.40	0.16	73697.14	0.42
310 (0.02 mm)		7.3881	0	74005.5	0

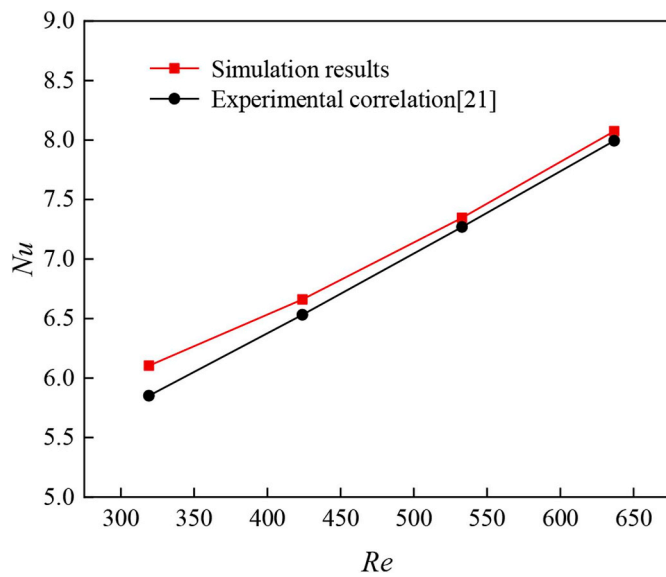


Fig. 2. Comparison of simulation results with experimental data of Liu et al. [16].

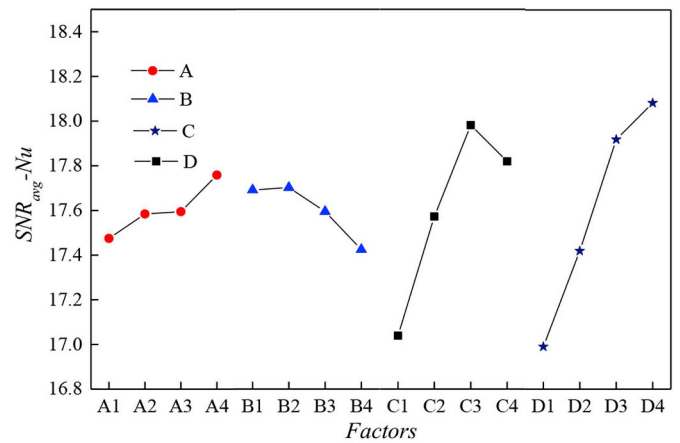
number are less than 5%. Therefore, the numerical method is considered reliable.

3. Taguchi method

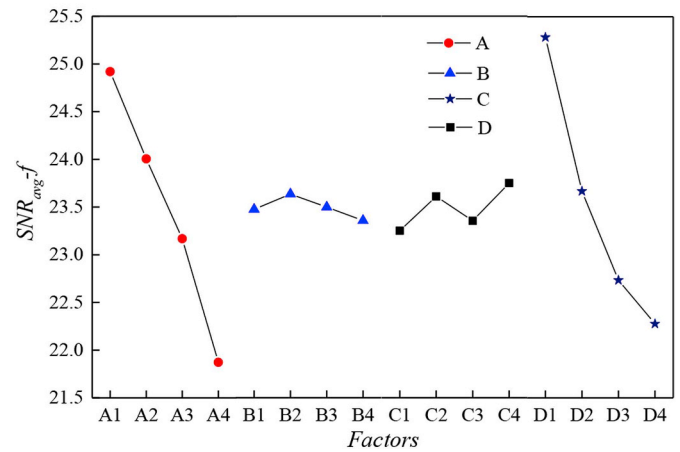
The Taguchi method was used to optimize the design and improve the robustness of the product. The Taguchi method can be used to design a series of factor combinations, according to the number and levels of impact factors. By analyzing the results of the experiments, an optimal impact factor combination can be obtained. In this work, the Taguchi method was employed to investigate the effect degree and optimize the structure of the LVGs.

3.1. Selection of influence factors and objectives

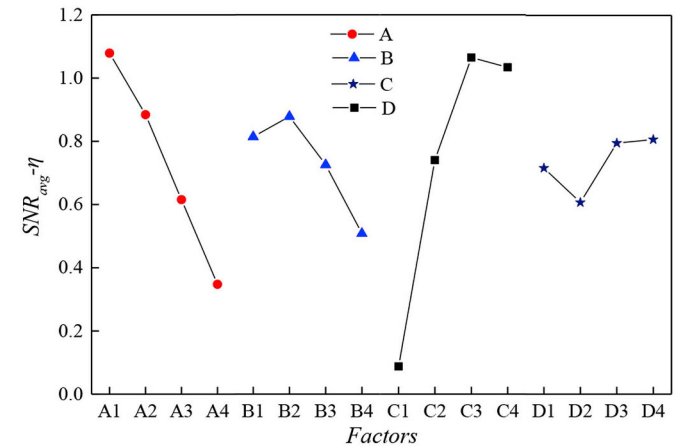
In the present study, Nusselt number and Fanning friction factor



(a) Nu



(b) f



(c) η

Fig. 3. Impact degree of geometric parameters on Nu , f , and η : (a) Nu , (b) f , and (c) η .

were adopted as the evaluation indexes of heat transfer and flow resistance, respectively. To evaluate the overall performance, the overall efficiency (η) was defined as [23,31,32].

Table 4
Levels of each factor with LVGs.

Levels	Factors (Code)			
	L (A) [length of LVGs (μm)]	b (B) [width of LVGs (μm)]	S _l (C) [longitudinal spacing (μm)]	N (D) [number of LVGs]
1	300	40	100	3
2	350	45	200	6
3	400	50	300	9
4	450	55	400	12

$$\eta = \frac{Nu/Nu_s}{(f/f_s)^{1/3}} \quad (10)$$

Hence, the objectives included Nusselt number, Fanning friction factor, and overall efficiency. Four impact factors, including the length (L) and width (b) of LVGs, longitudinal spacing (S_l) of LVGs, and number (N) of LVGs, and four levels in each impact factor, were considered, as shown in Table 4. The parameter values shown in Table 4 are determined according to Ref [21] and the requirement of Taguchi method. Also, the upper and lower value of the parameters are limited by the structure of the microchannel. Based on the theory underlying the Taguchi method, an orthogonal experiment with four factors and four levels, L₁₆ (4⁴), was designed as shown in Table 5.

3.2. Signal-to-noise ratio

Signal-to-noise Ratio (SNR) is an important parameter in the Taguchi method used to evaluate the robustness of a system. Generally, a large SNR is favorable for robustness. The optimal object is to get a large SNR for the evaluation indexes. However, for evaluation indexes in this paper, large Nu and overall efficiency, and small f are expected. So two definitions of the SNR were used [28]:

$$SNR_{lb} = -10 \lg \left(\frac{1}{n} \sum_{i=1}^n \frac{1}{Y_i^2} \right) \quad (11)$$

$$SNR_{sb} = -10 \lg \left(\frac{1}{n} \sum_{i=1}^n Y_i^2 \right) \quad (12)$$

where SNR_{lb} and SNR_{sb} are appropriate for the larger-the-better-type characteristics and smaller-the-better-type characteristics, respectively, Y is the value of the index and n represents the replicated experimental units which is one in this paper. Eq. (11) is applied to Nusselt number and the overall efficiency, and Eq. (12) is applied to friction factor. For example, when Eq. (11) is applied to calculate the SNR_{Nu}, the expression is shown as:

$$SNR_{Nu} = -10 \lg \left(\frac{1}{n} \sum_{i=1}^n \frac{1}{Nu^2} \right) \quad (13)$$

where, Nu is calculated by Eq. (4).

4. Results and discussions

Table 6 shows the numerical simulation results of orthogonal design and the SNR of Nu, f and η computed by Eq. (11) and Eq. (12).

Since there is more than one different factor between any two combinations, the data processing is necessary, and some parameters are defined. SNR_{avg} is the average SNR of same impact factor in the same level, which is defined as.

$$SNR_{avg}(i, j) = \frac{\sum_{k=1}^n SNR(i, j)}{n} \quad (14)$$

where i is the studied impact factor, j is the level of the factor and n is

Table 5
Orthogonal array of L₁₆ (4⁴).

Test number	Factor			
	A	B	C	D
1	1	1	1	1
2	1	2	2	4
3	1	3	3	2
4	1	4	4	3
5	2	2	1	2
6	2	1	2	3
7	2	4	3	1
8	2	3	4	4
9	3	3	1	3
10	3	4	2	2
11	3	1	3	4
12	3	2	4	1
13	4	4	1	4
14	4	3	2	1
15	4	2	3	3
16	4	1	4	2

Table 6
Simulation results.

Test number	Response and SNR					
	Nu	SNR _{Nu}	f	SNR _f	η	SNR _η
1	6.808	16.660	0.04903	26.191	1.0825	0.6885
2	7.879	17.930	0.06322	23.983	1.1511	1.2222
3	7.451	17.444	0.05527	25.150	1.1383	1.1253
4	7.820	17.865	0.06060	24.351	1.1587	1.2797
5	7.057	16.972	0.06201	24.151	1.0376	0.3208
6	7.709	17.740	0.06658	23.533	1.1069	0.8823
7	7.144	17.079	0.05282	25.544	1.1081	0.8918
8	8.459	18.546	0.07250	22.793	1.1806	1.4422
9	7.283	17.246	0.07769	22.193	0.9933	-0.0584
10	7.478	17.476	0.07025	23.067	1.0548	0.4632
11	8.490	18.578	0.08066	21.866	1.1435	1.1649
12	7.144	17.079	0.05282	25.545	1.1081	0.8918
13	7.309	17.278	0.09477	20.467	0.9330	-0.6020
14	7.197	17.143	0.06415	23.857	1.0463	0.3930
15	8.736	18.827	0.09057	20.860	1.1322	1.0782
16	7.751	17.787	0.07667	22.308	1.0618	0.5210

Table 7
CR of each factor for evaluation indexes.

Factors	CR		
	Nu	f	η
A	7.00	44.60	32.10
B	11.16	4.06	16.24
C	37.90	7.31	42.92
D	43.93	44.03	8.74

the number of cases in Table 5 which include the studied impact factor and the level.

The range (R) of each impact factor is selected to represent the ability of influence, which is defined as.

$$R_i = \max(SNR_{avg}(i, j)) - \min(SNR_{avg}(i, j)) \quad (15)$$

where i is the number of impact factors and j is the level of the factor. To represent the influence ratio clearly, the contribution ratio (CR) is defined as

$$CR(i) = \frac{R_i}{\sum_{i=1}^m R_i} \quad (16)$$

where m is the number of impact factors.

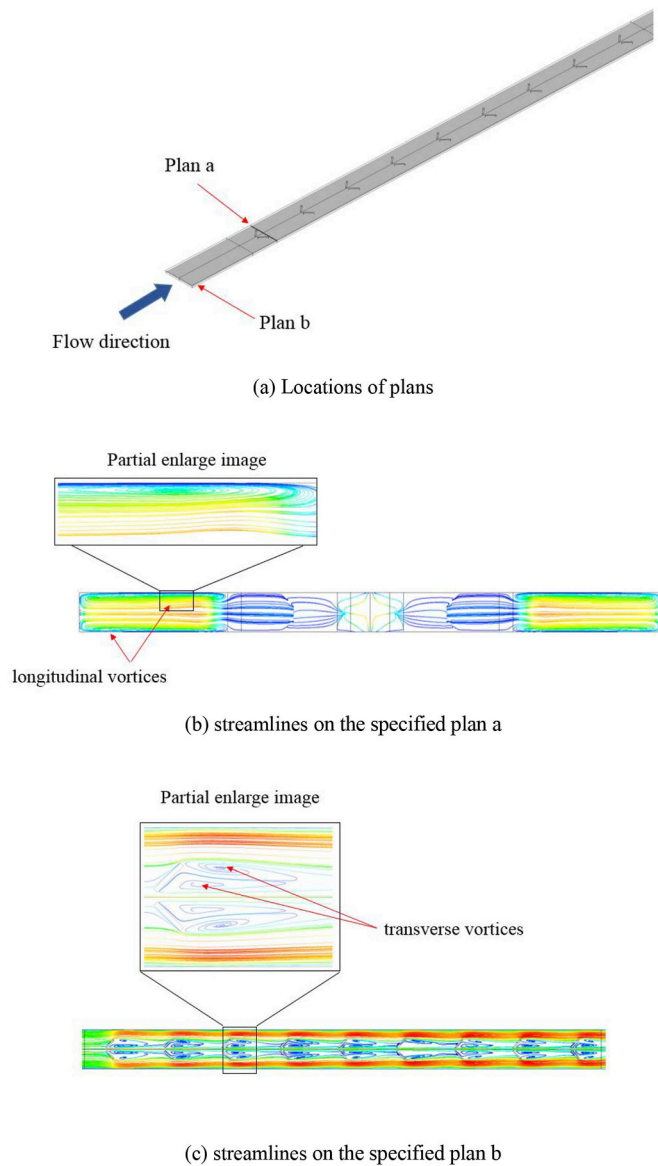


Fig. 4. Streamlines distribution on the specified plan: (a) Locations of plans and (b) streamlines on the specified plan a and (c) streamlines on the specified plan b.

4.1. Analysis of the Taguchi method

4.1.1. Analysis of impact degree

Based on the simulation results and calculation of SNR_{avg} , the factor-effect plot shown in Fig. 3 was obtained. Fig. 3(a) and (b)

represent the influence on Nusselt number and friction factor, respectively. From Fig. 3(a), it can be seen that the spacing and number of LVG pairs have a significant influence on Nusselt number. The reason is that increasing the number of LVGs pairs increases the heat-exchange area and generates more vortices that are beneficial for heat transfer. The spacing of the LVG pairs can, furthermore, influence the distribution of velocity. Table 7 shows the contribution ratio of the impact factors calculated by Eq. (16). Compared to the CR shown in Table 7, the impact degree of different impact factors is $D > C > B > A$ for Nusselt number. The sum of the contribution ratios of the longitudinal spacing and number of LVGs is more than 80%. Hence, the number and the spacing of the LVGs should be considered the main factors when optimizing the heat-transfer characteristics of microchannels.

As shown in Fig. 3(b), the length and number of LVGs have significant effects on the friction factor, because with increasing number of LVG pairs, more longitudinal vortices are generated, leading to more loss of resistance. Moreover, the projected area on the cross-section increases with increasing LVG length, which means that more fluid will be influenced. By comparing the CR shown in Table 7, the effect orders of different impact factors are $A > D > C > B$ for friction factor. The length and number of LVG pairs have a great influence on the friction factor, with CR of 44.6% and 44.0%, respectively.

Fig. 3(c) reveals that the length and spacing of LVG pairs have a significant effect on the overall efficiency, while the other factors have lower impacts. Regarding Nusselt number, the LVG spacing is the significant impact factor, while the influence of length is unremarkable. Conversely, the length of LVGs has a significant influence on friction factor, while the influence of spacing is insignificant. Although the number of LVG pairs both has the most significant influences on Nusselt number and friction factor, its impact on the overall efficiency is minimal. What's more, as shown in Table 7, the sum of the CR of the length and spacing of LVGs is 75.02%. Hence, the length and spacing of LVGs should be considered the main impact factors affecting overall efficiency.

4.1.2. Analysis of the mechanism of LVGs

In this section, the mechanism of LVGs and the influence of investigated parameters on heat transfer and flow resistance are analyzed. Fig. 4 shows the streamline distribution on the specified plans. Plan a is located at $z = 1.2$ mm. Plan b is located at half of the microchannel height ($y = 0.05$ mm). From Fig. 4(b), the longitudinal vortices generated by the LVGs can be observed. The two longitudinal vortices are located in the downstream of the flow direction. The longitudinal vortices can disturb the flow boundary layer which is beneficial for the fluid mixing and enhanced heat transfer. Also, as shown in Fig. 4(c), there are two transverse vortices behind each side of the LVGs pairs. The disturbance of the fluid in the region behind the longitudinal vortex is strengthened by the transverse vortices. Moreover, they also increased disturbance in the downstream region. However, the generation of the vortices also causes higher pressure losses.

Fig. 5 shows the influence of longitudinal spacing on velocity

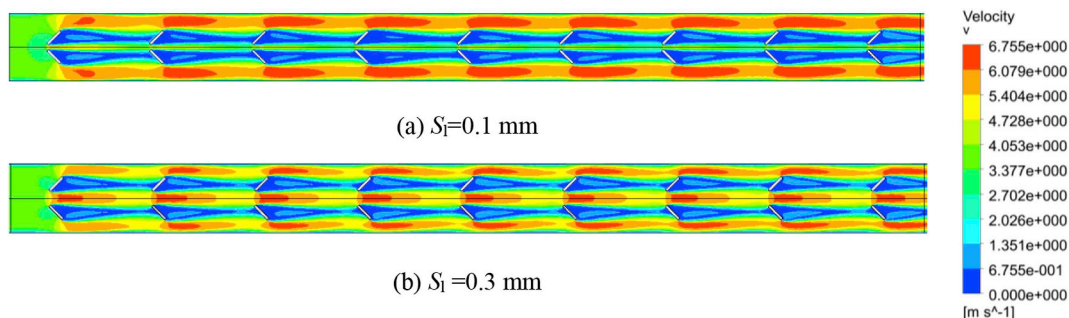


Fig. 5. Velocity distribution in specified plane b with different S_1 values: (a) $S_1 = 0.1$ mm and (b) $S_1 = 0.3$ mm.

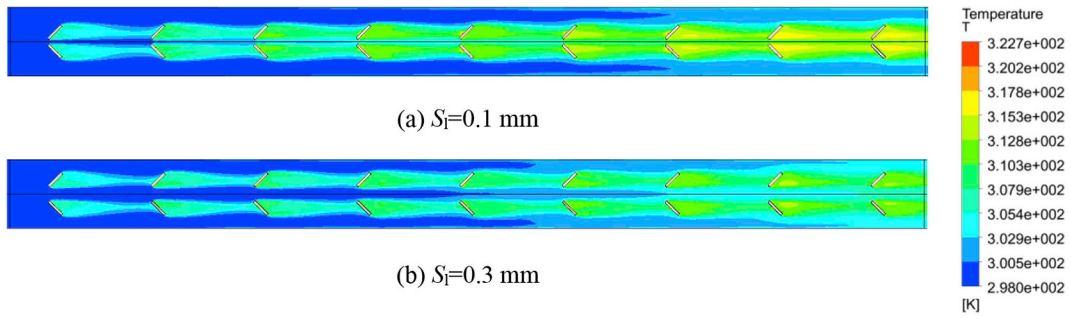


Fig. 6. Temperature distribution in specified plane b with different S_1 values: (a) $S_1 = 0.1$ mm and (b) $S_1 = 0.3$ mm.

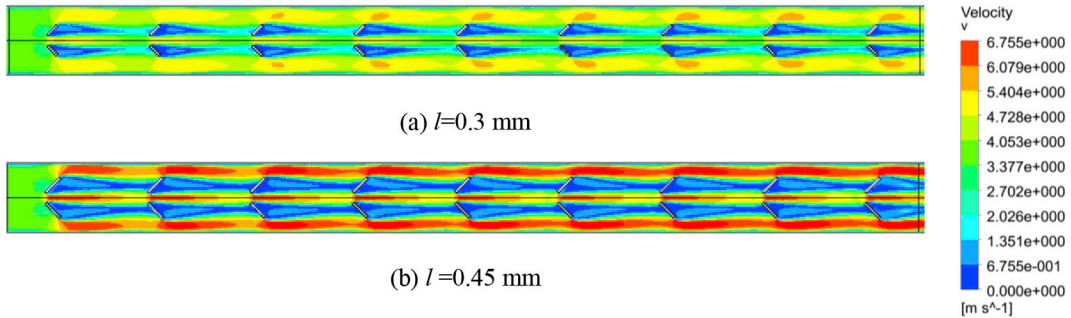


Fig. 7. Velocity Temperature distribution in specified plane b with different S_1 values: (a) $l = 0.3$ mm and (b) $l = 0.45$ mm.

distribution and Fig. 6 shows temperature distribution. It can be seen from Fig. 5 that the increase of spacing has a significant influence on the fluid flow of the microchannel combined with LVGs. In the case with small longitudinal spacing, because of the small flow area between the LVGs pairs, there is high fluid velocity zone in the region between the LVGs and the side wall of the microchannel, especially in the region of LVGs tail end in the direction of flow. In the case with large longitudinal spacing, it can be seen that the high-speed region also appears in the middle of the longitudinal vortex pair, which is more conducive

to fluid mixing. As shown in Fig. 6, increasing the longitudinal spacing of LVGs can facilitate better mixing of the high- and low-temperature fluids. In addition, the large longitudinal spacing of LVG pairs leads to better temperature uniformity in the outlet.

Fig. 7 shows the influence of length of LVGs on velocity distribution and Fig. 8 shows temperature distribution. The different influences of LVGs length on heat transfer and pressure drop can be demonstrated by comparing Fig. 7(a) and (b). From Fig. 7 it can also be seen that increasing the LVG length causes a large low-velocity-fluid region behind

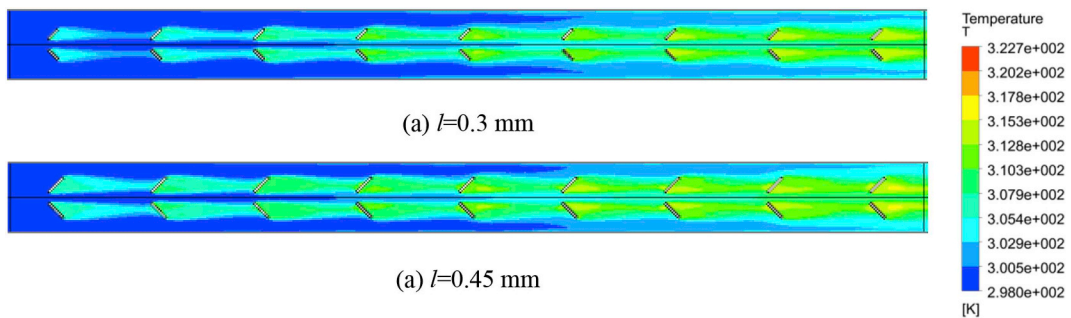


Fig. 8. Temperature distribution in specified plane b with different l values: (a) $l = 0.3$ mm and (b) $l = 0.45$ mm.

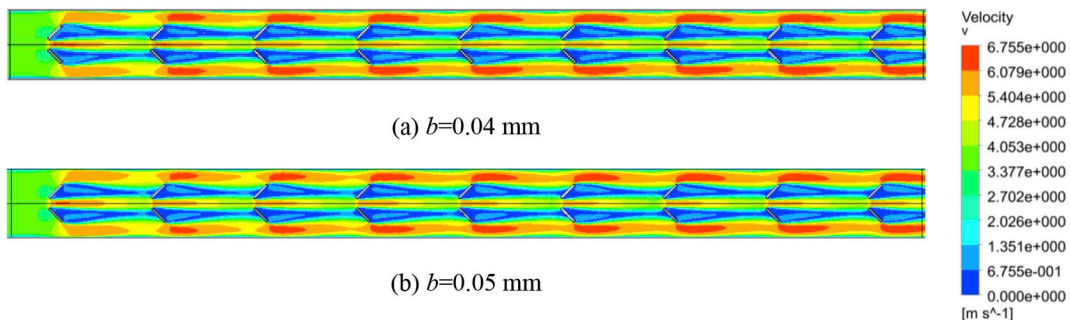


Fig. 9. Velocity Temperature distribution in specified plane b with different b values: (a) $b = 0.04$ mm and (b) $b = 0.05$ mm.

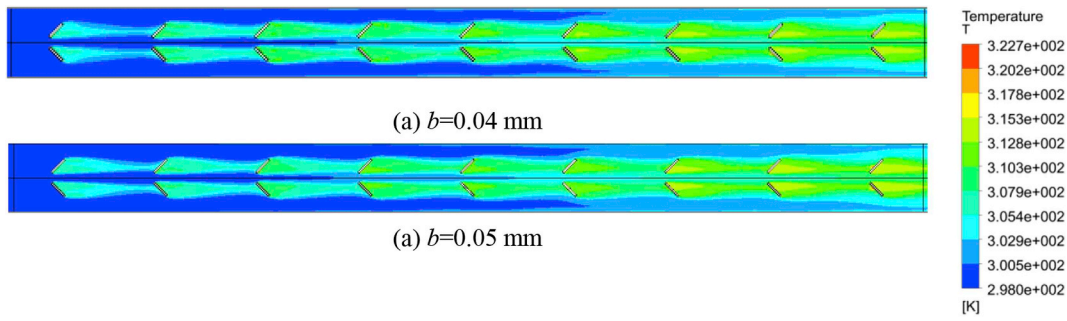


Fig. 10. Temperature distribution in specified plane b with different S_1 values: (a) $b = 0.04$ mm and (b) $b = 0.05$ mm.

Table 8
Comparison of optimized structure with original model.

Evaluation index	Original model	Optimized model	Difference (100%)
Nusselt number	7.31	9.03	23.6
Overall efficiency	1.09	1.18	7.2

Table 10
Parameter linear transformation.

Factors	Linear transformation expression $l_0 = 0.35$ mm, $b_0 = 0.045$ mm, $S_{10} = 0.2$ mm, $N_0 = 6$, $Re_0 = 253.5$ $\Delta l = 50$ mm $\Delta b = 5$ mm $\Delta S_1 = 0.1$ mm $\Delta N = 3$ $\Delta Re = 84.5$
l length of LVGs	$l = \frac{l-l_0}{\Delta l}$
B width of LVGs	$b = \frac{b-b_0}{\Delta b}$
S_l longitudinal spacing	$S_l = \frac{S_l-S_{10}}{\Delta S_1}$
N number of LVGs	$N = \frac{N-N_0}{\Delta N}$
Re Reynold number	$Re = \frac{Re-Re_0}{\Delta Re}$

Table 11
Coefficients of regression RSM.

Source	Nu	f	η
b_0	5.91	0.095	1
b_1	0.024	7.173E-003	-0.034
b_2	-0.019	-3.813E-004	-6.441E-003
b_3	0.045	-1.092E-003	0.017
b_4	-0.076	0.012	-0.044
b_5	0.44	-0.026	-0.063
$b_{1,2}$	0.018	1.303E-004	9.281E-003
$b_{1,3}$	0.031	-2.748E-004	-1.844E-003
$b_{1,4}$	0.023	2.723E-003	-0.016
$b_{1,5}$	0.031	-6.423E-004	-3.406E-003
$b_{2,3}$	-0.020	1.344E-004	-0.010
$b_{2,4}$	-0.023	3.212E-004	-0.011
$b_{2,5}$	-0.015	8.666E-005	-9.469E-003
$b_{3,4}$	+0.020	-3.536E-004	0.010
$b_{3,5}$	7.187E-003	4.691E-004	6.031E-003
$b_{4,5}$	0.021	-2.193E-003	0.012
$b_{1,1}$	2.307E-003	+4.776E-003	-0.019
$b_{2,2}$	-3.743E-003	-0.014	0.067
$b_{3,3}$	0.012	3.502E-003	-0.014
$b_{4,4}$	-0.057	3.519E-003	-0.022
$b_{5,5}$	-0.020	0.012	-6.517E-003

Table 9
Levels of each factor with LVGs for RSM.

Levels	Code of factors (actual value)				
	A	B	C	D	E
	[length of LVGs (μm)]	[width of LVGs (μm)]	[longitudinal spacing (μm)]	[number of LVGs]	Reynolds number
1	-1 (300)	-1 (40)	-1 (100)	-1 (3)	-1 (169)
2	0 (350)	0 (45)	0 (200)	0 (6)	0 (253)
3	1 (400)	1 (50)	1 (300)	1 (9)	1 (338)

the LVGs as well as a high-velocity-fluid region near the side wall of the microchannel, which increases the pressure drop obviously. However, as shown in Fig. 8, the differences of temperature distribution with various length are not obvious.

Fig. 9 and Fig. 10 present the influence of LVGs width on velocity distribution and temperature distribution, respectively. It can be seen that there is little difference of both velocity distribution and temperature distribution since the width of LVGs influenced the LVGs structure inconspicuously.

By the comprehensive comparison of Figs. 5–10, the impact degree

of factors can be explained. Comparing Figs. 5, 7 and 9, it can be seen that the velocity distribution depended on the length of LVGs strongly which means variations of length of LVGs can impact the pressure drop significantly. However, the variation of width influences the velocity distribution inconspicuous. Comparing Figs. 6, 8 and 10, it can be seen that the influence of the longitudinal space of LVGs on temperature distribution are significant while the influence of varying width is inconspicuous.

4.1.3. Optimal LVGs structure

Regarding the Nusselt number and overall efficiency factor, the optimization objective is to obtain the factor combinations that have the largest SNR. The levels of each impact factor showing the largest

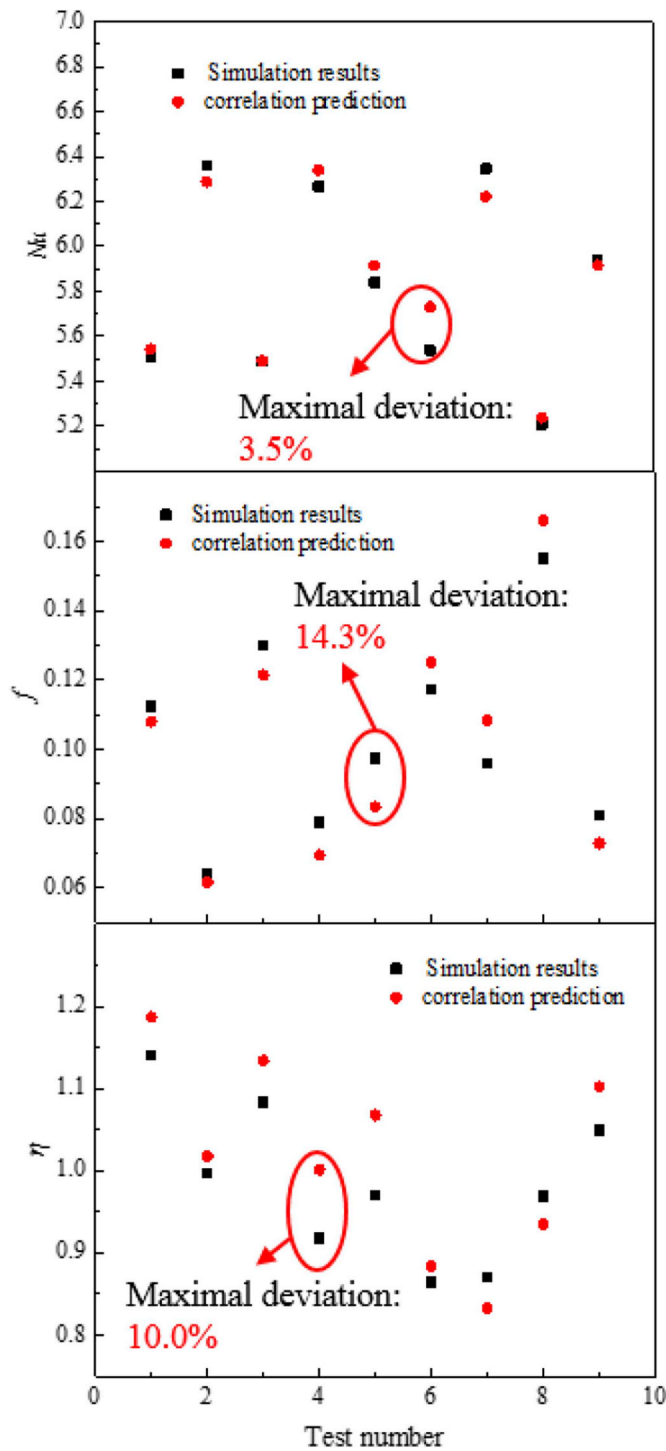


Fig. 12. Comparison of simulation results with correlation results.

SNR for Nu and f can be deemed as the level of optimal combinations for heat-transfer and overall characteristics, respectively [33]. It can be determined from Fig. 3 that the optimal impact factor combinations are A4B2C3D4 for Nusselt number and A1B2C3D4 for overall efficiency. Furthermore, the model “G2” in the literature [21], which shows good heat-transfer-enhancement performance, was chosen as the original model. Table 8 shows the verification of the optimal combination obtained. As presented in Table 8, the optimal structures improve by 23.6% and 7.2% for Nusselt number and overall efficiency, respectively, compared with the original model.

4.2. Regression analysis

4.2.1. Response surface methodology design

Although the Taguchi method can be used to analyze the impact degree of multiple parameters on object factors and obtain the optimal combinations, it is difficult to obtain the correlations between thermo-hydraulic performance and structure parameters. Furthermore, response surface methodology (RSM) is usually adopted to establish a multiple regression model to explain the influence of investigated factors on heat-transfer performance [34,35]. In this paper, central composite design (CCD), the most popular RSM design, is applied to the second-order model fitting. Fig. 4 shows the two-factor CCD model. Each CCD model contains factorial points, center points, and axial points. In Fig. 4, the red vertex of the square represents the factorial points which are used to fit linear and interaction terms. The star points represent the axial points which are used to estimate the quadratic terms. The value of α determines the position of the axial runs. Different α value means different CCD design.

The second-order multiple regression can be expressed as

$$Z = b_0 + \sum_{i=1}^{N-1} \sum_{j=i+1}^N (b_{i,j}X_iX_j) + \sum_{i=1}^N (b_{i,i}X_i^2) + \varepsilon \quad (17)$$

where Z represents the response factors; X is the impactor factors; b is the coefficient; N is the total number of impact factors and ε is the error term.

Considering the limitations of the microchannel structure, the face-centered design was adopted. In central composite face-centered design, the value of α shown in Fig. 11 is selected as one which means the axial points are in the face center of the cube. So the level of each factor is three (−1,0,1) for the face-centered design. The impact factors, codes and levels for RSM are given in Table 9.

To evaluate the accuracy of the model, analysis of variance (ANOVA) was carried out. P-values less than 0.05 indicate that the influence of the item is significant. In appendix A, it can be seen that the linear terms of C, D, and E are the significant model terms for Nu . Similar to the ANOVA of Nu , the linear terms of A, D, and E; interaction terms A•D and D•E; and quadratic terms B² and E² are the significant model terms for f . The linear terms of A and C, interaction terms D•E, and quadratic terms B² are the significant model terms for η .

4.2.2. Multiple regression model of responses

According to the analysis of the RSM, the second-order multiple regression correlations in dimensionless form between impact parameters and Nu , f , and η can be obtained. To satisfy the dimensionless requirement and unify parameters variation range, the linear transformation of model parameters as shown in Table 10 is carried out. The correlations are expressed as follows:

$$Y = b_0 + b_1 \cdot l + b_2 \cdot b + b_3 \cdot S_l + b_4 \cdot N + b_5 \cdot Re + b_{1,2} \cdot l \cdot b + b_{1,3} \cdot l \cdot S_l + b_{1,4} \cdot l \cdot N + b_{1,5} \cdot l \cdot Re + b_{2,3} \cdot b \cdot S_l + b_{2,4} \cdot b \cdot N + b_{2,5} \cdot b \cdot Re + b_{3,4} \cdot S_l \cdot N + b_{3,5} \cdot S_l \cdot Re + b_{4,5} \cdot N \cdot Re + b_{1,1} \cdot l^2 + b_{2,2} \cdot b^2 + b_{3,3} \cdot S_l^2 + b_{4,4} \cdot N^2 + b_{5,5} \cdot Re^2, \quad (18)$$

where the coefficients of each term of the regression model are presented in Table 11. The correlation can be used to predict the values of Nu , f , and η within the range of the present study. As shown in Table 11, the influence of terms on evaluation indexes are reflected on the value of the coefficients. It can be seen that for the linear terms, the number of LVGs and Reynolds number have a considerable influence on the heat transfer and flow resistance. It is evident that there are differences on the order of magnitudes among these coefficients as shown in Table 11. The models are not sensitive to those items which have a small order of

magnitude coefficients. Moreover, the full-form second regression model is very complex and not convenient for application. Hence, the items which P-values less than 0.5 according to the ANOVA are removed from the correlations to simplify the correlations. The simplified correlations are expressed as follows:

$$Nu = b_0 + b_1 \cdot l + b_2 \cdot b + b_3 \cdot S_l + b_4 \cdot N + b_5 \cdot Re + b_{1,2} \cdot l \cdot b + b_{1,3} \cdot l \cdot S_l + b_{1,4} \cdot l \cdot N + b_{1,5} \cdot l \cdot Re + b_{2,3} \cdot b \cdot S_l + b_{2,4} \cdot b \cdot N + b_{2,5} \cdot b \cdot Re + b_{3,4} \cdot S_l \cdot N + b_{4,5} \cdot N \cdot Re + b_{4,4} \cdot N^2, \tag{19}$$

$$f = b_0 + b_1 \cdot l + b_3 \cdot S_l + b_4 \cdot N + b_5 \cdot Re + b_{1,4} \cdot l \cdot N + b_{1,5} \cdot l \cdot Re + b_{4,5} \cdot N \cdot Re + b_{1,1} \cdot l^2 + b_{2,2} \cdot b^2 + b_{3,3} \cdot S_l^2 + b_{4,4} \cdot N^2 + b_{5,5} \cdot Re^2, \tag{20}$$

$$\eta = b_0 + b_1 \cdot l + b_2 \cdot b + b_3 \cdot S_l + b_4 \cdot N + b_5 \cdot Re + b_{1,2} \cdot l \cdot b + b_{1,4} \cdot l \cdot N + b_{2,3} \cdot b \cdot S_l + b_{2,4} \cdot b \cdot N + b_{2,5} \cdot b \cdot Re + b_{3,4} \cdot S_l \cdot N + b_{3,5} \cdot S_l \cdot Re + b_{4,5} \cdot N \cdot Re + b_{2,2} \cdot b^2 + b_{4,4} \cdot N^2, \tag{21}$$

where, the coefficients of the simplified correlation are contained within Table 10. To verify the accuracy of the simplified correlation, nine new test cases which are not employed to the second-order model fitting are simulated. The comparison of simulation and correlation results was carried out and the results are shown in Fig. 12. Over the range of test cases, the maximum differences between value predicted by the correlations and simulation results are less than 5%, 15% and 10% for Nusselt number, friction factor, and overall efficiency,

Appendix A. Analysis of variance (ANOVA)

Table A1 shows the ANOVA results for the response surface quadratic model. In Table A1, SS denotes the sum of squares, df the degree of freedom, and F the value of F-distribution. P is calculated by the value of F-distribution.

Table A1
ANOVA results for Nu, f, and η.

Source	Nu				f			η		
	df	SS	F	P	SS	F	P	SS	F	P
A	1	0.020	2.60	0.1175	1.794E-003	65.73	< 0.0001	0.039	19.28	0.0001
B	1	0.012	1.55	0.2226	5.765E-006	0.21	0.6493	1.411E-003	0.70	0.4094
C	1	0.068	8.66	0.0063	3.812E-005	1.40	0.2469	9.522E-003	4.73	0.0380
D	1	0.20	25.34	< 0.0001	4.520E-003	165.56	< 0.0001	0.066	32.74	< 0.0001
E	1	6.66	853.96	< 0.0001	0.024	861.09	< 0.0001	0.13	66.21	< 0.0001
A•B	1	0.011	1.39	0.2473	3.125E-008	1.145E-003	0.9732	2.757E-003	1.37	0.2515
A•C	1	0.030	3.89	0.0581	1.531E-006	0.056	0.8144	1.088E-004	0.054	0.8178
A•D	1	0.016	2.10	0.1581	2.365E-004	8.66	0.0063	8.288E-003	4.12	0.0517
A•E	1	0.032	4.04	0.0539	1.378E-005	0.50	0.4831	3.713E-004	0.18	0.6708
B•C	1	0.013	1.68	0.2049	1.531E-006	0.056	0.8144	3.465E-003	1.72	0.1999
B•D	1	0.016	2.11	0.1570	2.531E-006	0.093	0.7629	3.894E-003	1.93	0.1749
B•E	1	7.503E-003	0.96	0.3349	7.812E-007	0.029	0.8668	2.869E-003	1.42	0.2423
C•D	1	0.013	1.69	0.2036	3.781E-006	0.14	0.7125	3.424E-003	1.70	0.2025
C•E	1	1.653E-003	0.21	0.6488	9.031E-006	0.33	0.5696	1.164E-003	0.58	0.4532
D•E	1	0.014	1.81	0.1891	1.488E-004	5.45	0.0267	4.729E-003	2.35	0.1362
A•A	1	1.632E-005	2.092E-003	0.9638	6.235E-005	2.28	0.1415	8.481E-004	0.42	0.5214
B•B	1	3.822E-005	4.898E-003	0.9447	5.185E-004	18.99	0.0002	0.011	5.59	0.0249
C•C	1	3.603E-004	0.046	0.8314	3.066E-005	1.12	0.2980	4.519E-004	0.22	0.6392
D•D	1	8.158E-003	1.05	0.3150	3.066E-005	1.12	0.2980	1.145E-003	0.57	0.4568
E•E	1	9.825E-004	0.13	0.7253	3.283E-004	12.03	0.0017	1.051E-004	0.052	0.8209

References

[1] D.B. Tuckerman, R.F.W. Pease, High-performance heat sinking for VLSI, IEEE

respectively. From the validation, the correlations presented is considered to be reliable.

5. Conclusions

Based on the present work, the following conclusions can be drawn.

- (1) According to intuitive analysis, the number and spacing of the LVG pairs have the dominant impact on Nusselt number. The length and number of LVG pairs have a high CR for the friction factor. In the range of parameters investigated, the length and spacing of LVGs have a significant influence on overall performance.
- (2) The optimal impact factor combinations for Nusselt number and overall efficiency were determined using the Taguchi method. The optimal structures for Nusselt number and overall efficiency increased by 23.6% and 7.2%, respectively, compared with the original model.
- (3) The reliable dimensionless correlations for Nu, f, and η were established based on analysis of the RSM. Moreover, the correlation results have good coherence with simulation results over the range of cases tested especially for Nusselt number and overall efficiency.

Acknowledgments

This work was supported by the National Natural Science Foundation of China (Grant No. 51576155), the Foundation for Innovative Research Groups of the National Natural Science Foundation of China (No.51721004) and the Fundamental Research Funds for the Central Universities.

Electron. Device Lett. 2 (5) (1981) 126–129.
 [2] E.G. Colgan, B. Furman, M. Gaynes, et al., A practical implementation of silicon microchannel coolers for high power chips, IEEE Trans. Compon. Packag. Technol. 30 (2) (2007) 218–225.

- [3] X.F. Peng, G.P. Peterson, Convective heat transfer and flow friction for water flow in microchannel structures, *Int. J. Heat Mass Transf.* 39 (12) (1996) 2599–2608.
- [4] W. Qu, I. Mudawar, Experimental and numerical study of pressure drop and heat transfer in a single-phase micro-channel heat sink, *Int. J. Heat Mass Transf.* 45 (12) (2002) 2549–2565.
- [5] C.Y. Zhao, T.J. Lu, Analysis of microchannel heat sinks for electronics cooling, *Int. J. Heat Mass Transf.* 45 (24) (2002) 4857–4869.
- [6] K.C. Toh, X.Y. Chen, J.C. Chai, Numerical computation of fluid flow and heat transfer in microchannels, *Int. J. Heat Mass Transf.* 45 (26) (2002) 5133–5141.
- [7] X.D. Wang, B. An, J.L. Xu, Optimal geometric structure for nanofluid-cooled microchannel heat sink under various constraint conditions, *Energy Convers. Manag.* 65 (2013) 528–538.
- [8] L. Lin, J. Zhao, G. Lu, et al., Heat transfer enhancement in microchannel heat sink by wavy channel with changing wavelength/amplitude, *Int. J. Therm. Sci.* 118 (2017) 423–434.
- [9] L. Chuan, X.D. Wang, T.H. Wang, et al., Fluid flow and heat transfer in micro-channel heat sink based on porous fin design concept, *Int. Commun. Heat Mass Transf.* 65 (2015) 52–57.
- [10] S.L. Wang, X.Y. Li, X.D. Wang, et al., Flow and heat transfer characteristics in double-layered microchannel heat sinks with porous fins, *Int. Commun. Heat Mass Transf.* 93 (2018) 41–47.
- [11] L. Lin, Y.Y. Chen, X.X. Zhang, et al., Optimization of geometry and flow rate distribution for double-layer microchannel heat sink, *Int. J. Therm. Sci.* 78 (2014) 158–168.
- [12] C. Leng, X.D. Wang, T.H. Wang, An improved design of double-layered micro-channel heat sink with truncated top channels, *Appl. Therm. Eng.* 79 (2015) 54–62.
- [13] W.A. Khan, M.M. Yovanovich, J.R. Culham, Optimization of microchannel heat sinks using entropy generation minimization method, *Twenty-Second Annual IEEE Semiconductor Thermal Measurement and Management Symposium. IEEE*, 2006, pp. 78–86.
- [14] S.J. Kim, D. Kim, Forced convection in microstructures for electronic equipment cooling, *J. Heat Transf.* 121 (3) (1999) 639–645.
- [15] M.K. Moharana, G. Agarwal, S. Khandekar, Axial conduction in single-phase simultaneously developing flow in a rectangular mini-channel array, *Int. J. Therm. Sci.* 50 (2011) 1001–1012.
- [16] M.K. Moharana, G. Agarwal, S. Khandekar, Axial conduction in single-phase simultaneously developing flow in a rectangular mini-channel array, *Int. J. Therm. Sci.* 50 (6) (2011) 1001–1012.
- [17] R. Chein, J. Chuang, Experimental microchannel heat sink performance studies using nanofluids, *Int. J. Therm. Sci.* 46 (1) (2007) 57–66.
- [18] M. Zeng, L.H. Tang, M. Lin, et al., Optimization of heat exchangers with vortex-generator fin by Taguchi method, *Appl. Therm. Eng.* 30 (13) (2010) 1775–1783.
- [19] Y.L. He, Y. Zhang, Advances and outlooks of heat transfer enhancement by longitudinal vortex generators, *Elsevier, Adv. Heat Transfer* 44 (2012) 119–185.
- [20] A. Lemouedda, M. Breuer, E. Franz, et al., Optimization of the angle of attack of delta-winglet vortex generators in a plate-fin-and-tube heat exchanger, *Int. J. Heat Mass Transf.* 53 (23–24) (2010) 5386–5399.
- [21] C. Liu, J. Teng, J.C. Chu, et al., Experimental investigations on liquid flow and heat transfer in rectangular microchannel with longitudinal vortex generators, *Int. J. Heat Mass Transf.* 54 (13–14) (2011) 3069–3080.
- [22] C. Chen, J.T. Teng, C.H. Cheng, et al., A study on fluid flow and heat transfer in rectangular microchannels with various longitudinal vortex generators, *Int. J. Heat Mass Transf.* 69 (2014) 203–214.
- [23] A. Ebrahimi, E. Roohi, S. Kheradmand, Numerical study of liquid flow and heat transfer in rectangular microchannel with longitudinal vortex generators, *Appl. Therm. Eng.* 78 (2015) 576–583.
- [24] A. Datta, D. Sanyal, A.K. Das, Numerical investigation of heat transfer in micro-channel using inclined longitudinal vortex generator, *Appl. Therm. Eng.* 108 (2016) 1008–1019.
- [25] A. Datta, A.K. Das, P. Dey, et al., Multi-objective optimization of laminar heat transfer and friction factor in rectangular microchannel with rectangular vortex generators: an application of NSGA-II with gene expression programming metamodel, *J. Heat Transf.* 139 (7) (2017) 072401.
- [26] J.F. Zhang, Y.K. Joshi, W.Q. Tao, Single phase laminar flow and heat transfer characteristics of microgaps with longitudinal vortex generator array, *Int. J. Heat Mass Transf.* 111 (2017) 484–494.
- [27] G. Taguchi, *Taguchi on Robust Technology Development: Bringing Quality Engineering Upstream*, ASME, New York, 1993.
- [28] J.S. Leu, Y.H. Wu, J.Y. Jang, Heat transfer and fluid flow analysis in plate-fin and tube heat exchangers with a pair of block shape vortex generators, *Int. J. Heat Mass Transf.* 47 (19–20) (2004) 4327–4338.
- [29] J.M. Wu, W.Q. Tao, Numerical study on laminar convection heat transfer in a rectangular channel with longitudinal vortex generator. Part A: verification of field synergy principle, *Int. J. Heat Mass Transf.* 51 (5–6) (2008) 1179–1191.
- [30] J.M. Wu, W.Q. Tao, Numerical study on laminar convection heat transfer in a channel with longitudinal vortex generator. Part B: parametric study of major influence factors, *Int. J. Heat Mass Transf.* 51 (13–14) (2008) 3683–3692.
- [31] Y.L. Zhai, G.D. Xia, X.F. Liu, et al., Heat transfer in the microchannels with fan-shaped reentrant cavities and different ribs based on field synergy principle and entropy generation analysis, *Int. J. Heat Mass Transf.* 68 (2014) 224–233.
- [32] M. Khoshvaght-Aliabadi, O. Sartipzadeh, A. Alizadeh, An experimental study on vortex-generator insert with different arrangements of delta-winglets, *Energy* 82 (2015) 629–639.
- [33] H. Wang, Y. Liu, P. Yang, et al., Parametric study and optimization of H-type finned tube heat exchangers using Taguchi method, *Appl. Therm. Eng.* 103 (2016) 128–138.
- [34] H.Z. Han, B.X. Li, H. Wu, et al., Multi-objective shape optimization of double pipe heat exchanger with inner corrugated tube using RSM method, *Int. J. Therm. Sci.* 90 (2015) 173–186.
- [35] S. Chamoli, P. Yu, S. Yu, Multi-objective shape optimization of a heat exchanger tube fitted with compound inserts, *Appl. Therm. Eng.* 117 (2017) 708–724.